EPJ B
Condensed Matter and Complex Systems
EPJ.org
your physics journal

Eur. Phys. J. B (2015) 88: 317 DOI: 10.1140/epjb/e2015-60695-x

Chladni figures at the nanoscale

Christophe Taillan, Nicolas Combe and Joseph Morillo

edp sciences
Società Italiana di Fisica
Springer

Eur. Phys. J. B (2015) 88: 317
DOI: 10.1140/epjb/e2015-60695-x

THE EUROPEAN PHYSICAL JOURNAL B

Regular Article

Chladni figures at the nanoscale

Christophe Taillan[1,2], Nicolas Combe[1,2,a], and Joseph Morillo[1,2]

[1] Centre d'Elaboration de Matériaux et d'Études Structurales, CNRS UPR 8011, 29 rue J. Marvig, BP 94347, 31055 Toulouse Cedex 4, France
[2] Université de Toulouse, UPS, 31055 Toulouse, France

Received 25 August 2015 / Received in final form 13 October 2015
Published online 2 December 2015 –

Abstract. On a substrate submitted to a standing surface acoustic wave, an adatom diffuses and preferentially locates in the vicinity of anti-nodes of the transversal displacements of the wave. Using molecular dynamics simulations, the physical mechanism yielding this structuration is revealed: the adatom is mainly driven by the time-varying longitudinal displacement field of the wave. Besides, the intensity of the structuration as a function of the substrate temperature and of the amplitude, direction and frequency of the wave is studied.

1 Introduction

To grow nano-structures during any atomic deposition process, the structuration techniques obviously present some great advantages compared to the time-consuming and expensive lithography stages. However, the control of the spatial and size distribution of nanostructures using structuration techniques is a challenging task. The most studied structuration techniques are the use of dislocation networks [1], the surface patterning of the substrate [2] and the well-known Stranski-Krastanov method [3], an extensively studied technique that takes advantage of the elastic properties of both deposited and substrate materials.

To improve the control of the spatial and size distribution of nanostructures during the growth, an alternative structuration technique has been recently proposed [4].

Such proposition was inspired from a well-known experiment at the macro-scale: a sand bunch dropped on a metallic plate excited in resonance self-organizes and forms the so-called Chladni figures [5]. This structuring effect has been transposed at the nano-scale: a standing surface acoustic wave (StSAW) drives the adatom diffusion on a defectless substrate and leads to the structuration of adatoms on the surface.

In reference [4], this structuring effect was evidenced through large scale molecular dynamics (MD) simulations of an adatom diffusion on the (001) surface of a fcc crystal with the presence of a StSAW in the [100] direction: the spatial probability distribution of the adatom is significantly increased in the vicinity of the anti-nodes of the wave (transverse) displacement (or equivalently the nodes of the longitudinal displacement). The basis of a theoretical interpretation of this structuring effect was also given through the derivation, from a Langevin type equation, of an effective time independent potential whose minima correspond to the antinodes of the StSAW transverse displacement field. A complete theoretical description was then reported in reference [6] where, from a full atomic scale description of an adatom diffusion in one dimension, a generalized Langevin equation was analytically derived and was then studied in detail. Its solutions were reported in reference [7].

In this manuscript, performing a MD study, the structuring effect of a StSAW on an adatom diffusion on a (001) fcc surface is thoroughly analysed. This includes detailed analyses of the physical mechanism leading to the structuring effect and of the role of temperature, and of the StSAW amplitude, frequency and wave vectors directions on the structuring effect. While MD results for a [100] StSAW have been presented in reference [4], the present manuscript presents results for the [110] StSAW, compares both results and discusses the role of the wave vector direction.

Section 2 details the model and the technical issues of the MD simulations. Section 3 investigates the structuring effect induced by the StSAW propagating in the [110] directions on the diffusion of an adatom on a (001) surface of a fcc crystal. In Section 4, the physical origin of the structuration introduced in Section 3 is studied in detail. Finally, the last section is devoted to the study of the influence of the amplitude, frequency and direction of the StSAW and of the temperature on the structuring effect.

2 Simulation details

The diffusion of a single adatom on a (001) fcc surface submitted to a unidimensional StSAW in the [110] directions is considered. Large scale classical MD simulations

[a] e-mail: combe@cemes.fr

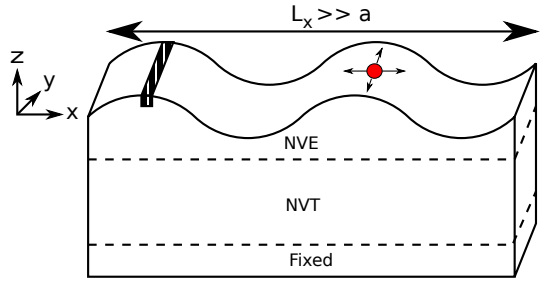

Fig. 1. Sketch of the simulation model. The adatom (red disk) is diffusing on the upper surface. Atoms in the dashed region have an imposed vertical sinusoidal displacement (frequency Ω) and produce a StSAW along the x direction. The atoms of the 12 upper layers of the substrate are in the microcanonical ensemble (NVE). The atoms in the large intermediate region are thermostated (NVT ensemble) and the 4 bottom layers of the substrate are kept fixed.

with periodic boundary conditions are performed using the LAMMPS code [8]. Figure 1 reports a sketch of the simulation cell. The substrate, with dimensions L_x, L_y and L_z, is a fcc (001) slab normal to the z direction of the simulation cell, with the adatom on the upper surface. The simulation cell size in the z direction is fixed from the cutoff distance of the interaction potential to avoid any interaction between the slab and its z periodic images. Similarly, L_y is fixed to ensure that any atom does not interact with its own y images.

The StSAW (wave-vector along the x direction) is generated by imposing a periodic displacement $z(t)$ along the z direction to a few atoms: these atoms, displayed in a dashed region in Figure 1 belong to the 3 top layers of the substrate and to three adjacent x planes:

$$z(t) = z_{eq} + A\cos(\Omega t), \tag{1}$$

with z_{eq} their equilibrium positions, A and Ω, the amplitude and angular frequency of the StSAW. As a result, two identical Rayleigh waves (surface waves) with wavelength λ and propagating along the x and $-x$ directions are generated. The StSAW is obtained by adjusting the frequency Ω of the displacement so that L_x is a multiple of λ. Thus, due to the periodic boundary conditions in the x direction, the two Rayleigh waves interfere to form the StSAW. To prevent any misunderstanding of the effects induced by the substrate crystalline structure and by the StSAW on the adatom diffusion, the StSAW wavelength is chosen so that $\lambda \gg a$, with a the substrate lattice parameter. The calculations presented in Section 3 were made with $\lambda = 17\,a_x$, with a_x the lattice parameter in the x direction and $L_x = 2\lambda$. The wavelength is then typically of the order of a few nanometers. Other values of λ will be considered in Section 6 by changing the StSAW frequency. In all cases, this leads to L_x values large enough to avoid any interaction between an atom and its x periodic images. The x directions, the StSAW wave-vector direction is along the [110] substrate crystal direction. Finally, L_z is chosen of the order of magnitude of the characteristic attenuation length of the StSAW in the substrate, e.g. roughly λ [9]. Nevertheless, to prevent any induced overall motion of the system in the z direction, the 4 bottom layers of the slab are kept fixed. In doing so, we indeed tend to simulate a semi-infinite crystal in the $-z$ direction.

The resulting dimensions of the substrate L_x, L_y and L_z are respectively $34\,a_x$, $4\,a_y$ and $15.5\,a$ (31 atomic layers) and $a_x = a_y = \sqrt{2}\,a$ for the [110] StSAW. With these choices, the simulation box typically contains about 24 000 atoms.

The StSAW generation process results in a continuous injection of energy in the system corresponding to the work of the force necessary to impose the time dependent displacement of the previously defined group of atoms close to the top surface. To prevent the induced uncontrolled temperature increase of the system, a Nose-Hoover thermostat (NVT ensemble) is applied. However, in order to avoid any unphysical consequences on the interaction process between the adatom and the StSAW, top layers are not coupled to the thermostat. The adatom as well as the atoms in the 12 top layers are in the microcanonical ensemble. Only, the layers between the 12 top and the 4 bottom layers are submitted to the Nose-Hoover thermostat. In doing so, the 12 top layers are naturally thermallized by the underlying crystal.

The amplitude of the StSAW is chosen to induce an elastic deformation and to avoid any plastic deformation or loss of crystallinity of the substrate, noticeably at the maximum amplitude displacement of the wave: typically, the amplitude A varies from about $0.06\,a$ to $0.31\,a$ for $\lambda = 17\,a_x$. Note that the relevant quantity to avoid any plastic deformation is the local deformation and not the amplitude of the displacement field: the range of values of A will then be extended when longer wavelengths will be considered in Section 6.

As already reported [4], the structuring effect induced by the StSAW on the diffusion of the adatom is not sensitive to the choice of the semi-empirical potential describing the atomic interactions. Hence, due to its cheap computational cost, the present study will be entirely performed using the same Lennard-Jones potential as in our initial study [4]:

$$E_{\text{pair}} = 4\epsilon\left[\left(\frac{\sigma}{r}\right)^{12} - \left(\frac{\sigma}{r}\right)^{6}\right], \tag{2}$$

with

- $\sigma_{ss} = 1.0$, $\epsilon_{ss} = 1.0$ between substrate atoms (mass $m_s = 1.0$),
- $\sigma_{as} = 1.0$, $\epsilon_{as} = 0.82$ between the adatom (mass $m_a = 1.0$) and the substrate atoms.

Based on this choice of parameters for the substrate-substrate interactions, distances, masses, energies, times, and temperatures are expressed respectively in units of σ_{ss}, m_s, ϵ_{ss}, $\sqrt{\frac{m_s\sigma_{ss}^2}{\epsilon_{ss}}}$ and ϵ_{ss}/k_B (k_B the Boltzmann constant) in the following.

A 2.63 cut-off distance with a polynomial switching function is applied to smoothly truncate the Lennard-Jones potential beyond the 13th neighbour shell. The LJ

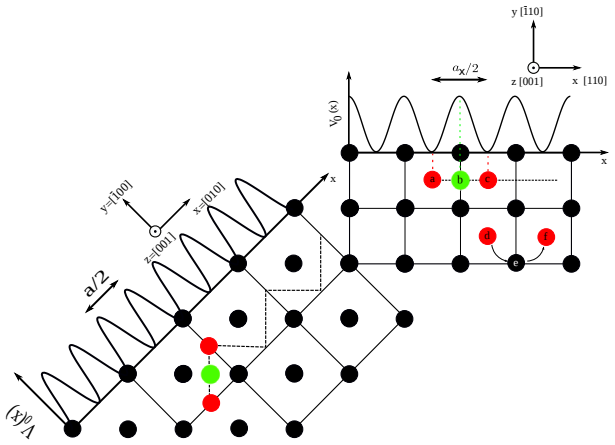

Fig. 2. Top view of the upper substrate (001) surface layer and sketch of $V_0(x)$, the unperturbed crystalline potential felt by the adatom as a function of its position x for a [100] (bottom left) and [110] (top right) StSAW. Red (a and c) adatoms illustrate the stable positions of the crystalline potential while green (b) positions illustrate the saddle points of the diffusion mechanism. d, e and f sites illustrate an exchange mechanism: adatom d pushes out a substrate atom e that becomes an adatom on the substrate at position f. Dashed lines illustrate the most direct diffusion pathway (minimum path way) in the x direction.

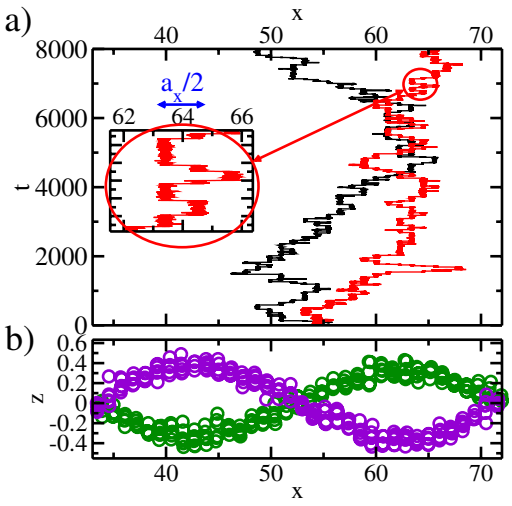

Fig. 3. (a) x-positions (abscissa) as a function of time (ordinate) of an adatom diffusing on a (001) substrate surface without (black) and with (red) a [110] StSAW. Inset: zoom on the trajectory. (b) z-positions of the atoms of the top layer of the substrate at two different times separated by half a period of the wave and corresponding to maxima of substrate transverse displacements. Simulations are performed using a Lennard-Jones interaction potential at the substrate temperature $T = 0.24$. The [110] StSAW parameters are: $A = 0.4$, $\Omega = 0.924$, $\lambda = 17a_x$.

parameters were chosen to avoid the evaporation of the adatom and the exchange mechanism on the simulation time-scale. The evaporation interrupts the diffusion for obvious reasons. Figure 2 illustrates an exchange mechanism on the (001) surface between the adatom d and the substrate atom e: the adatom d pushes out the substrate atom e that becomes an adatom on the substrate at position f. The occurrence of this phenomenon increases with temperature or surface strain [10]. The exchange mechanism is not desired here since it yields the diffusion of substrate atoms on the substrate surface.

Typical simulation times are of the order of 4 million steps of 2×10^{-3} time units. These simulation times correspond to a few nanoseconds with σ_{ss}, m_s and ϵ_{ss} values corresponding to fcc noble metals.

3 Dynamic structuring effect

In this section we evidence the structuring effect of a [110] StSAW on an adatom diffusing on a (001) fcc substrate surface.

3.1 Single trajectory

The trajectory of a single adatom diffusing on the (001) substrate surface submitted to a [110] StSAW at the temperature $T = 0.24$ (corresponding typically to 1000 K for a noble metal) is investigated. The amplitude and angular frequency of the StSAW are $A = 0.4$ (LJ distance unit) and $\Omega = 0.924$ (LJ angular frequency unit) for the [110] StSAW. With these parameters, the adatom diffuses on significant lengths on the simulation time-scale while the evaporation and exchange mechanisms are very limited.

Figure 3b reports the extremal transversal displacement of the substrate top layer atoms, at two different times separated by half a period of the [110] StSAW. Nodes and anti-nodes of the transverse displacements are clearly evidenced (nodes at $x \approx 33, 52, 71$ and anti-nodes at $x \approx 42$ or 62 on Fig. 3b).

Figure 3a reports the trajectories, the x-position (abscissa) as a function of time (ordinate) of an adatom diffusing on the (001) surface with (red) and without (black) the presence of the [110] StSAW. On the substrate without StSAW, the adatom standardly has a Brownian-like motion. Besides, the trajectory of the adatom on the substrate with the StSAW seems to be confined in the vicinity of anti-nodes of vibration. These results suggest a structuring effect of the StSAW on the adatom diffusion. Such a structuring effect can be evidenced using a statistical analysis as we did in reference [4]. The histogram $H(x)$ of the x-coordinate of the diffusing adatom is measured from 200 independent trajectories of 8000 time units long, with initial positions evenly spread along one wavelength of the StSAW. Parameters of the simulations are identical to the ones of Figure 3. Since the system is invariant by translation of length λ, rather than reporting $H(x)$, the histogram $P(x)$ defined by $P(x) = H(x \bmod \lambda)$ where mod designs the modulo is reported. Finally, $P(x)$ is normalized following $\int_0^\lambda P(x)dx = 1$.

Figures 4a and 4b report the histogram $P(x)$ without (black) and with (red) the [110] StSAW while Figure 4c reports the same quantity as Figure 3b.

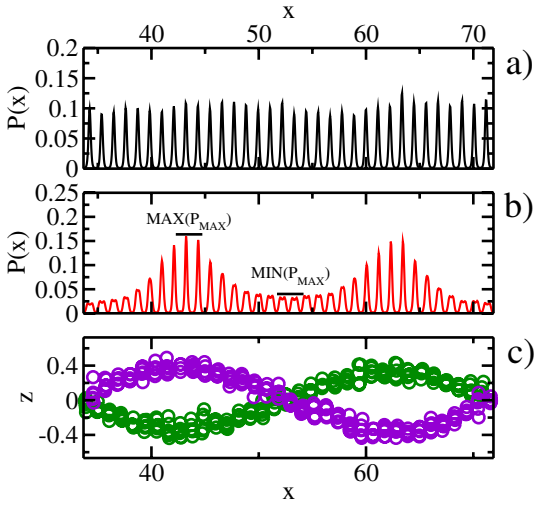

Fig. 4. (a), (b) Distributions $P(x)$ of adatoms positions diffusing on a (001) surface (a) without and (b) with the [110] StSAW. (c) Same as Figure 3b. Distributions are calculated from 200 independent trajectories of 8000 time units with initial conditions evenly spread along one wavelength of the StSAW. Simulations are performed using a Lennard-Jones interaction potential at the substrate temperature $T = 0.24$. The [110] StSAW parameters are: $A = 0.4$, $\Omega = 0.924$, $\lambda = 17a_x$.

Without StSAW in Figure 4a, $P(x)$ is an oscillating function of nearly constant amplitude. The oscillations occur with a $a_x/2$ periodicity. Indeed, the adatom diffuses through the crystalline potential $V_0(x)$ generated by the (001) surface substrate, whose minima are spaced every $a_x/2$ in the x direction ([110] direction) in agreement with Figure 2, reporting a schematic top view of the substrate surface as well as a sketch of the crystalline potential. The distance between minima of $V_0(x)$ can also be evidenced on the adatom trajectory as shown in the inset of Figure 3a: the adatom spends a significant time oscillating in the minima of this potential. The nearly constant amplitude of the oscillations of $P(x)$ in Figure 4a are related to the nearly Brownian trajectories of the adatom: the adatom has the same probability to be in any minimum of the crystalline potential. The fluctuations of the amplitude of $P(x)$ are due to the limited statistics used to calculate $P(x)$.

The average resident time τ_{diff}^{MD} of the adatom in a crystalline potential well is roughly $\tau_{diff}^{MD} = 50$ from a statistical analysis of the trajectory reported in Figure 3. Comparing this time to the StSAW period $T_{StSAW}^{MD} = \frac{2\pi}{\Omega} \approx 6.8$, the diffusion of the adatom in presence of the StSAW is far from the stochastic resonance condition [11].

In the presence of the [110] StSAW, $P(x)$, reported in Figure 4b is an oscillating function whose amplitude is spatially modulated with a $\lambda/2$ period. Again, the oscillations occur on a $a_x/2$ scale and are reminiscent of the crystalline potential. The amplitude of the oscillations varies on a length-scale $\lambda/2$ with maxima corresponding to anti-nodes of transverse substrate displacement. From Figure 4b, the probability to find an adatom in the vicinity of the anti-nodes is about 4 times greater than the one in the vicinity of a node: the structuring role of the StSAW is unambiguously evidenced.

It is worth noting that minima of $P(x)$ in Figure 4b can also be used to get some information on the diffusion process: indeed, the minima of $P(x)$ should be related to the dynamics of the adatom diffusion, i.e. to an effective activation barrier for the diffusion.

These results are very similar to the ones found for an adatom diffusing in the presence of a [100] StSAW (Fig. 2b of Ref. [4]). Hence, the structuring effect seems to be a physical phenomenon whose existence is independent on the StSAW wave direction (though its intensity can depend on the wave direction).

3.2 Force acting on the adatom

The StSAW succeeds to induce a structuring effect on the diffusion of the adatom. Therefore the wave induces an effective structuring force on the adatom. To identify and characterize this force, MD simulations are performed with an adatom confined successively in each of the potential wells along the wavelength of the StSAW. In order to constrain the ad-atom to remain in its initial well during the whole simulation time, the MD simulations are performed at low temperature $T = 0.05$. The residence time in a given crystalline potential well is strongly increased at low temperature. Note that the parameters of the MD simulations are identical to those of Figures 3 and 4 except for the temperature $T = 0.05$ and for the angular StSAW frequency $\Omega = 0.986$ which needed to be changed in order to adjust λ to the $T = 0.05$ lattice parameter ($\lambda = 17a_x$). With these parameters, the adatom is confined in its $t = 0$ crystalline potential well all along the MD trajectory of 650 time units.

The x-component $F_{tot}(X_n = n\ a_x/2, t)$ of the total force acting on the adatom (position $x(t)$ at time t) in the potential well at position $X_n = n\ a_x/2$ (n an integer) is recorded as a function of time t and spectrally analyzed for different values of $X_n = n\ a_x/2$. X_n designs here the position of the potential wells of the unperturbed crystalline potential in which the adatom is confined during the MD trajectory. Note that the force $F_{tot}(X_n = n\ a_x/2, t)$ involves all the forces that act on the adatom and not only the force induced by the StSAW.

Figure 5 reports a typical example of the frequency dependence of the time Fourier transform $\tilde{F}_{tot}(X_n, \omega)$ of $F_{tot}(X_n = na_x/2, t)$ corresponding to the trajectory of an adatom in the potential well at $X_n = 15.6$: whereas the different features at high frequency ($\omega \geq 3$) are due to the thermal agitation, a huge peak, at $\omega = \Omega = 0.986$, the angular StSAW frequency, is clearly visible.

The whole ω and X_n variations of $\tilde{F}_{tot}(X_n, \omega)$ are reported on Figure 6a for the [110] StSAW, evidencing the existence of the peak at $\Omega = 0.986$ for all potential wells, with a spatial modulation at the StSAW wavelength λ.

This spatial modulation is visible on Figure 6b which reports $\tilde{F}_{tot}(X_n, \omega = \Omega)$ as a function of X_n as well as the transversal displacement of the substrate top layers (Figs. 6c). The $\tilde{F}_{tot}(X_n, \Omega)$ is modulated at the StSAW

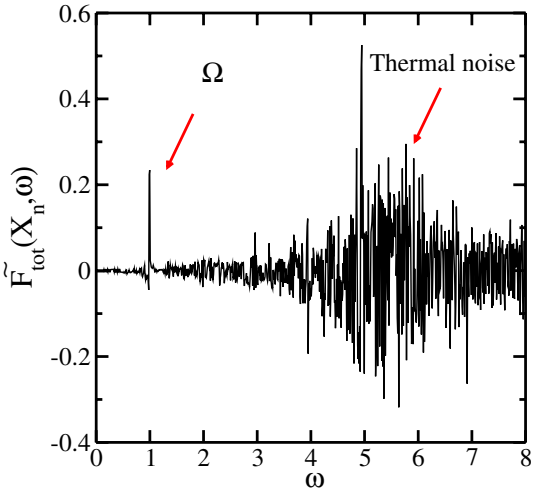

Fig. 5. Fourier transform $\tilde{F}_{tot}(X_n,\omega)$ of the x-component of the force $F_{tot}(X_n,t)$ at $X_n = 15.6$. The substrate temperature is $T = 0.05$. The StSAW is propagating along the [110] direction on the (001) surface with parameters: $A = 0.4$, $\Omega = 0.986$, $\lambda = 17a_x$.

wavelength λ and, its phase ϕ_{acc} is such that the nodes of the force correspond to the anti-nodes of the substrate transverse displacement field. $\tilde{F}_{tot}(X_n,\Omega)$ is thus the main contribution to the effective structuring force induced by the StSAW on an adatom in the potential well X_n.

These results are again very similar to ones obtained for an adatom diffusing in the presence of a [100] StSAW [4]. In the following, $F_{acc}(x,t)$ refers to the periodic force acting on an adatom at position x located in a crystalline potential well X_n at the StSAW frequency: this force thus corresponds to the Fourier component of $F_{tot}(X_n,t)$ at the StSAW frequency.

$$F_{acc}(x,t) = \tilde{F}_{tot}(X_n,\Omega)\cos(\Omega t), \quad (3)$$

$$= F^0_{acc}\sin(kX_n + \phi_{acc})\cos(\Omega t), \quad (4)$$

where $k = \frac{2\pi}{\lambda}$ and Ω are the StSAW wave vector and angular frequency and F^0_{acc} the amplitude of the spatial modulation of $\tilde{F}_{tot}(X_n,\Omega)$.

As we will show below, this force results from two contributions. The first one, that we call static, is the force $F_{StSAW}(x,t)$ induced by the StSAW that the adatom will experience if it is at rest at position x. This force is studied in detail in Section 4. The second one, that we will call dynamic, and revealed in Section 5 results from the ad-atom oscillating displacement induced by the StSAW in its crystalline potential well.

3.3 Quantifying the structuration

The structuring effect induced by the StSAW can be quantified. To this aim, the results reported in Figure 4 in terms of normalized histograms $P(x)$ can be consider on an energy scale by defining $\mathfrak{F}(x) = -kT\ln P(x)$. Due to the StSAW, the system is time-dependent, and thus $\mathfrak{F}(x)$

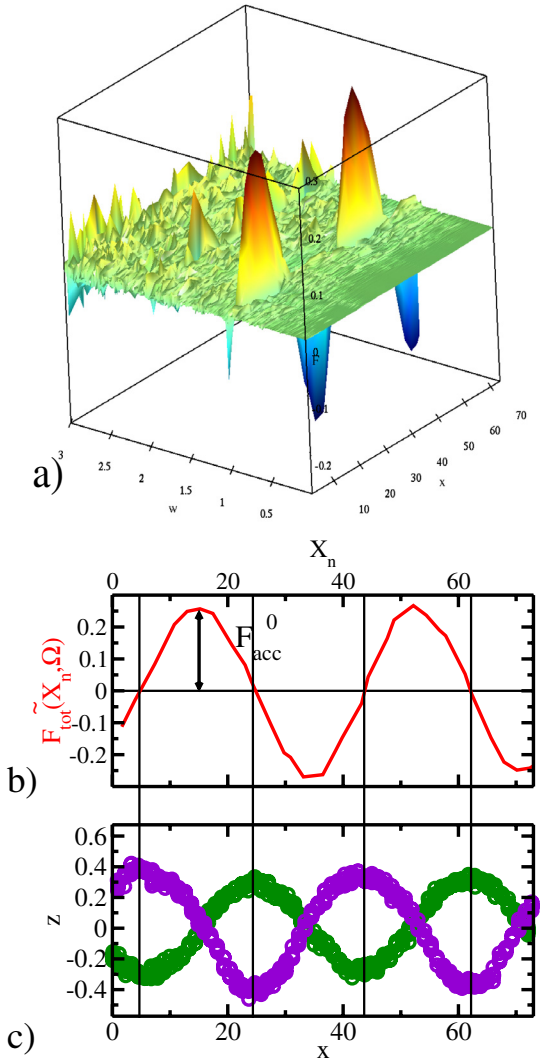

Fig. 6. (a) Fourier transform $\tilde{F}_{tot}(X_n,\omega)$ as a function of angular frequency ω and potential well position X_n. (b) Fourier component (red) $\tilde{F}_{tot}(X_n,\Omega)$ at excitation frequency $\Omega = 0.986$ as a function of the potential well position. (c) Same as Figure 3b. The substrate temperature is $T = 0.05$. The StSAW is propagating along the [110] direction on the (001) surface with parameters: $A = 0.4$, $\Omega = 0.986$, $\lambda = 17a_x$.

cannot be directly interpreted as a free energy. However, we suggest that $\mathfrak{F}(x)$ is related to the free energy of the system describing the slow variation of the adatom motion [4,7]. To quantify the structuring effect, the structuring energy $\Delta E^{\text{eff}}_{StSAW}$ is defined:

$$\frac{\Delta E^{\text{eff}}_{StSSAW}}{kT} = \ln\left(\frac{\text{MAX}(P_{\max})}{\text{MIN}(P_{\max})}\right), \quad (5)$$

where MAX (MIN) is the maximum (minimum) of the sets $P_{\max}$ of local maxima of $P(x)$. Figure 4 pictures the quantities $\text{MAX}(P_{\max})$ and $\text{MIN}(P_{\max})$. The structuring energy will be used below in order to reveal the physical mechanism responsible of the StSAW force and to compare the structuring effect dependence on the StSAW parameters.

4 Origin of the static force

In this section, the physical mechanisms leading to the existence of the static force $F_{StSAW}(x,t)$ induced by the StSAW that the ad-atom will experience if it is at rest at position x and acting on the adatom are described. The forces acting on the adatom are provided by the substrate, the only system that interacts with the adatom. As a consequence, the fundamental origin of the static force $F_{StSAW}(x,t)$ is the modulation of the interatomic potential between the substrate and the adatom by the displacement/strain field induced by the wave. Calling $\phi_{StSAW}(\boldsymbol{r},t)$ and $\phi_0(\boldsymbol{r})$ the crystalline potential seen by the adatom in the presence and absence of the StSAW, the static force simply writes:

$$\boldsymbol{F}_{StSAW}(\boldsymbol{r},t) = -\boldsymbol{\nabla}\left[\phi_{StSAW}(\boldsymbol{r},t) - \phi_0(\boldsymbol{r})\right]. \quad (6)$$

This expression is coherent with our former analytical work using an unidimensional model of the adatom motion [6]. In this section, we will first describe the displacement and strain fields induced by the StSAW in the substrate. Then the induced modifications of the crystalline potential seen by the adatom will be described. Finally, the induced modifications mainly responsible of the structuring effect will be revealed.

4.1 Displacement and strain fields induced by a StSAW

The displacement and strain fields induced by the StSAW are described in this section. Solving the Navier equation (linear elasticity theory) in a semi-infinite $z \leq 0$ medium [9], and assuming for simplicity the isotropy of the elastic properties of this medium, the displacement field $\boldsymbol{u}(x,z,t)$ in the xz plane of the substrate induced by a standing Rayleigh wave propagating in the x direction with angular frequency Ω and wave number k writes with the appropriate x and t origins:

$$u_x(x,z,t) = -\left(kbe^{\chi_l z} + \chi_t a e^{\chi_t z}\right)\sin(kx)\cos(\Omega t), \quad (7a)$$
$$u_z(x,z,t) = \left(\chi_l b e^{\chi_l z} + ka e^{\chi_t z}\right)\cos(kx)\cos(\Omega t), \quad (7b)$$

where

$$\chi_l = \sqrt{k^2 - \frac{\Omega^2}{c_l^2}}, \quad \chi_t = \sqrt{k^2 - \frac{\Omega^2}{c_t^2}},$$

with c_t and c_l the transverse and longitudinal sound speeds. Free boundary conditions at the free substrate surface[1] yield a relation between constants a and b and the dispersion relation :

$$2a\chi_t k + b\left(k^2 + \chi_t^2\right) = 0, \quad (8)$$
$$4\chi_t\chi_l k^2 = \left(k^2 + \chi_t^2\right)^2. \quad (9)$$

[1] $\bar{\bar{\sigma}}(x, z = 0, t).\boldsymbol{n} = 0$ $\forall t$ and $\forall x$ with $\bar{\bar{\sigma}}$ the stress tensor and $\boldsymbol{n}$, a unit vector perpendicular to the surface.

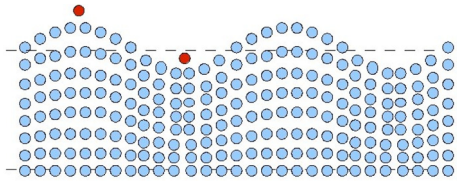

Fig. 7. Sketch of the substrate atoms positions in the presence of a StSAW at a time corresponding to maxima of the transverse displacement field.

Equation (9) is the dispersion relation for the surface acoustic wave (the angular frequency being hidden in χ_t and χ_l).

From equations (7)−(9) the displacement field at the substrate surface writes:

$$u_x(x, z = 0, t) = \sqrt{\frac{\chi_t}{\chi_l}} A \sin(kx)\cos(\Omega t), \quad (10a)$$
$$u_z(x, z = 0, t) = A\cos(kx)\cos(\Omega t), \quad (10b)$$

with $A = ka(1 - \frac{\sqrt{\chi_t\chi_l}}{k})$ the amplitude of the transverse displacement field.

Focusing on the spatial dependence along x, the longitudinal $u_x(x, z = 0, t)$ and transverse $u_z(x, z = 0, t)$ displacement fields at the substrate surface have a spatial quadrature phase relationship: this result evidenced for a StSAW propagating in an isotropic medium, can be extended to anisotropic media [12]. From equation (10a), the longitudinal strain field $\varepsilon_{xx}(x, z = 0, t)$ at the substrate surface reads:

$$\varepsilon_{xx}(x, z = 0, t) = \sqrt{\frac{\chi_t}{\chi_l}} Ak\cos(kx)\cos(\Omega t). \quad (11)$$

$\varepsilon_{xx}(x, z = 0, t)$ is spatially in-phase with the transversal displacement field $u_z(x, z = 0, t)$: this typically corresponds to the intuitive sketch reported in Figure 7 in which the distances between neighboring atoms are stretched at the maxima of the transverse displacement and compressed at the minima.

4.2 Qualitative analysis: modifications of the crystalline potential

The distance between successive substrate atoms depends at the first order on the longitudinal strain field and at the second order on the transverse strain field. Hence, the crystalline potential seen by the adatom essentially depends on the longitudinal displacement field of the substrate.

The mathematical expression of the force $F_{StSAW}(x,t)$ has been previously established in the scope of an unidimensional model [6]. We focus here on the physical mechanisms inducing the modification of the crystalline potential by the StSAW longitudinal displacement field and at the origin of $F_{StSAW}(x,t)$. We artificially decompose these modifications in three main physical mechanisms, which relative weight will be evaluated in Section 4.3.

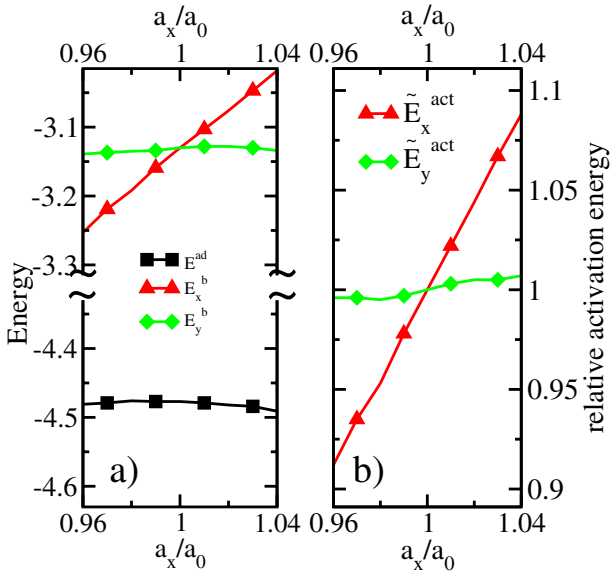

Fig. 8. (a) Adsorption energies E^{ad} (square black) and bridge energies E_x^{b} (triangle red) and E_y^{b} (diamond green) as a function of the relative lattice parameter a_x/a_0 in the [110] direction. (b) Relative diffusion barriers $\tilde{E}_x^{\mathrm{act}}$(triangle red) and $\tilde{E}_y^{\mathrm{act}}$(diamond green) as a function of the relative lattice parameter a_x/a_0.

4.2.1 Modulation of the adsorption and bridges sites, and diffusion barrier energies

The variations, with an applied strain field, of the adsorption and saddle point energies for surface diffusion is a well known phenomenon [13,14]. We have calculated these variations in the Lenard Jones potential model. The substrate is homogeneously strained in the [110] direction (x direction) (StSAW propagation direction), while the lattice parameter in the y direction is kept fixed to its equilibrium value $a_y = a_0$.

The resulting variations of the adsorption energy E^{ad} and the bridge sites energies E_x^{b} and E_y^{b} as a function of a_x/a_0 have been calculated with a_x the strained lattice parameter in the x direction. The strain field $\epsilon_{xx} = a_x/a_0 - 1$ was varied from -4% to $+4\%$ (of the same order as the maximal longitudinal strain field imposed in the MD simulations). The bridge sites energies were calculated using the Nudge Elastic Band (NEB) method [15] between two configurations corresponding to the adatom in two adjacent fcc sites, either in the x or y directions. Figures 8a and 8b report, as a function of a_x/a_0 with $x = [110]$, the calculated adsorption energy E^{ad} and bridge sites energies E_x^{b} and E_y^{b}, and the resulting normalized diffusion barriers

$$\tilde{E}_{x/y}^{\mathrm{act}} = \frac{E_{x/y}^{\mathrm{act}}}{E_0^{\mathrm{act}}} = \frac{E_{x/y}^{\mathrm{b}} - E^{\mathrm{ad}}}{E_{x/y,0}^{\mathrm{b}} - E^{\mathrm{ad}}},$$

with $E_{x/y,0}^{\mathrm{b}}$ the bridge sites energy for $a_x = a_0$.

The adsorption energy E^{ad} and the bridge energy in the y direction E_y^{b} weakly depend on a_x/a_0 (i.e. on the substrate strain ϵ_{xx}), whereas the bridge site energy in the x direction E_x^{b} strongly depends on it: it linearly increases with a_x/a_0. As a result, the diffusion barriers in the x and y directions have a very different response to the longitudinal substrate strain field ϵ_{xx}. In the direction of propagation of the StSAW, the normalized diffusion barrier $\tilde{E}_x^{\mathrm{act}} = E_x^{\mathrm{act}}/E_0^{\mathrm{act}}$ linearly increases with a_x/a_0, a linear regression giving $\tilde{E}_x^{\mathrm{act}} - 1 = 2.2(a_x/a_0 - 1)$. Whereas in the perpendicular direction it weakly depends on it (Fig. 8b), a linear regression giving $\tilde{E}_y^{\mathrm{act}} - 1 = 0.14(a_x/a_0 - 1)$.

In order to compare these results with the former ones using a StSAW wave propagating in the [100] direction [4], the same study has been performed for a [100] StSAW and results are qualitatively similar to the one described above: the adsorption energies weakly depend on a_x/a_0 while the bridge energies (note that all bridges sites are equivalent with this lattice orientation cf. Fig. 1) linearly increase with a_x/a_0, roughly 0.0146 energy unit per 1% of the strain field ϵ_{xx}. The normalized diffusion barrier has hence a linear dependence $\tilde{E}^{\mathrm{act}} - 1 \approx 0.98(a_x/a_0 - 1)$.

In addition, since we also evidenced the structuring effect induced by a StSAW using a semi-empirical potential based on the Embedded Atom Method (EAM) for silver [4], a similar study has been conducted with this Ag EAM potential for a StSAW propagating in the [100] direction [16]. It was found that the diffusion energy barriers vary in the same way, but for different reasons: E_x^{b} and E_y^{b} are found to weakly depend on a_x/a_0, whereas E^{ad} linearly decreases with a_x/a_0 (roughly 16 meV per 1% of the strain field ϵ_{xx}).

Hence, for both Lenard-Jones and silver EAM potentials, the StSAW is expected to weakly modify the diffusion of the adatom along the direction normal to the direction of propagation of the wave (y), but may potentially significantly affect it along the direction of propagation (x).

4.2.2 Curvature effects

The longitudinal strain field (Eq. (10a)) by modifying the curvature of the crystalline potential seen by the adatom in each crystalline potential well modifies the three eigenangular frequencies ω_0^α ($\alpha \in \{1,2,3\}$) of the adatom trajectory in this well. To investigate this effect, MD simulations of an adatom oscillating around its equilibrium position in the crystalline potential well on a (001) surface of a frozen substrate are performed. Trajectories (10^5 steps) of the adatom are Fourier transform to get the angular-frequencies ω_0^α ($\alpha \in \{1,2,3\}$). The lattice parameter a_x along the x direction ([110]) was varied from $a_x/a_0 = 0.96$ to 1.04, while a_y ([$\bar{1}$10]) is fixed to its equilibrium value $a_y = a_0$. The adatom oscillations in the x, y and z directions are found to be decoupled, each one providing an angular-frequency, ω_0^α with $\alpha \in \{x,y,z\}$. This decoupling is indeed expected since, due to the symmetry of the system, the principal Hessian directions are expected to be the x, y, and z directions. Figure 9 reports

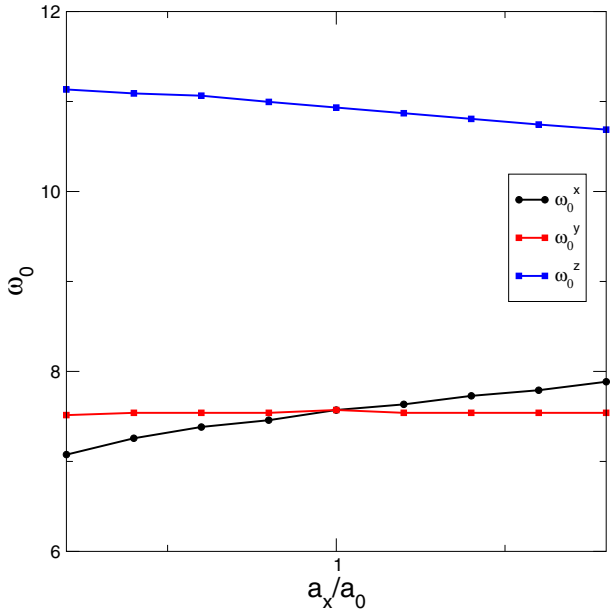

Fig. 9. Angular Eigen-frequencies of an adatom in a crystalline potential well as a function of the relative lattice parameter a_x/a_0.

the variations of the corresponding angular-frequencies as a function of the normalised substrate lattice parameter a_x/a_0. ω_0^y weakly depends on the lattice parameter, whereas ω_0^x and ω_0^z present an opposite weak linear dependence: a longitudinal strain change of $+1\%$ results in a relative frequency change of approximately $+1.5\%$ (-1.5%) in the x (z) directions. Thus, the motion of the adatom in the in-plane direction normal to the direction of propagation of the StSAW is weakly affected by it. In the out of surface direction (z), as one could intuitively expect, the softening (hardening) of the potential associated to an increase (decrease) of the interatomic spacing in the x in-plane direction, results in a softening (hardening) of the oscillation frequency in the z direction. Surprisingly, the effect of the longitudinal strain field is opposite in the direction of the strain field. Though counter-intuitive, this dependence of ω_0^x as a function of the longitudinal strain field has been confirmed by direct calculations of the associated component of the Hessian matrix.

4.2.3 Inertial effect

As reported by equation (10a), the StSAW induces a longitudinal displacement field $u_x(x,t)$ in the substrate. The minima of the crystalline potential are thus displaced by this field, which directly produces a force on the adatom. This force can roughly be evaluated for an adatom in a crystalline potential well. Indeed, assuming that the displacement $u_x(x,t)$ is small compared to the lattice parameter, the crystalline potential in the presence of the StSAW $\phi_{StSAW}(\boldsymbol{r},t)$ can be expanded at the first order in $u_x(x,t)$ [6]. As a result, the component of the force equation (6) induced by the StSAW along the StSAW direction is proportional to the second derivative of the crystalline potential compared to the x position and to the displacement field. Writing this second derivative as the product of the adatom mass m times the squares angular frequencies ω_0^x of the adatom oscillation in the potential well, the component of the force induced by inertial effects along the StSAW direction will be proportional to $m\left(\omega_0^x\right)^2 u_x(x,t)$ with m the adatom mass. This force actually has the same temporal and spatial periodicity as the force exhibited in Section 3.2.

4.3 Dominant physical mechanism driving the structuring effect

In Section 4.2, the main modifications of the crystalline potential induced by the StSAW have been identified. In this section, the quantitative comparison of the structurations induced by these mechanisms is addressed in order to reveal the dominant mechanism responsible of the structuring effect. Note that this study aims first to explain our MD simulations results and thus adopts a different approach than other results from the litterature [17].

To this aim, an unidimensional model of the adatom diffusion previously introduced [6,7] is used: the adatom trajectory is solution of the following unidimensional Langevin equation:

$$\ddot{x} + \gamma\dot{x} = -\frac{\partial\phi_i}{\partial x}(x,t) + \zeta(t), \tag{12}$$

where x and $\phi_i(x,t)$ design the coordinate of the diffusing adatoms and the crystalline potential seen by the adatom eventually modified by the StSAW. For simplicity, masses are given in the adatom mass unity and retardation effects have been neglected. Phonons thermally activated in the substrate, responsible of the energy transfer between the adatom and the substrate in the absence of StSAW are taken into account through the friction coefficient $\gamma = 0.1$ and a stochastic force $\zeta(t)$ satisfying: $\langle\zeta(t)\rangle = 0$ and $\langle\zeta(t)\zeta(t+\tau)\rangle = 2D\delta(\tau)$ and $D = 0.0035$ (where $\langle.\rangle$ designs a ensemble average and δ is the Dirac distribution). Five crystalline potentials $\phi_i(x,t)$ with $i \in 0,1,2,3,4$ are investigated. $\phi_0(x,t)$ is a simplified model crystalline potential whereas $\phi_i(x,t)$ with $i = 1,2,3,4$ investigates one of the possible previously mentioned modifications induced by the StSAW independently from the others:

– the perfect unperturbed crystalline potential $\phi_0(x,t)$:

$$\phi_0(x,t) = V_0 \mathrm{Min}\left[\left(\xi^2 - \frac{\sigma^2}{4}\right), 0\right] \tag{13a}$$

with

$$x = X_n + \xi$$
$$X_n = na_x \quad \text{and} \quad -a_x/2 < \xi < a_x/2$$

with $\sigma = 0.6$, n an integer and $V_0 = 1$. $\mathrm{Min}[x,y]$ designs the smaller value of the set $\{x,y\}$. This crystalline potential is reported in Figure 10a as a function of x.

– $\phi_i(x,t)$ with $i \in \{1,2,3,4\}$ are analogous to the crystalline potential $\phi_0(x,t)$ equation (13) but minima values $E^{\rm ad}$ of $\phi_1(x,t)$, maxima values $E_x^{\rm b}$ of $\phi_2(x,t)$, the curvature in each potential well of $\phi_3(x,t)$ and the minima positions of $\phi_4(x,t)$ are spatially modulated at the StSAW wave vector and temporally at the StSAW frequency. Both spatial and temporal modulations are sinusoidal.

$$\phi_1(x,t) = \frac{V_0}{2}\mathrm{Min}\left[\left(\xi^2 - \frac{\sigma_{\rm eff}(x,t)^2}{4}\right), 0\right], \quad (14a)$$

with

$$\begin{aligned} x &= X_n + \xi, \\ X_n &= na_x \quad \text{and} \quad -a_x/2 < \xi < a_x/2, \\ \sigma_{\rm eff}(x,t) &= \sigma + \sigma_0 \cos(\Omega t)\cos(kX_n), \end{aligned} \quad (14b)$$

$$\phi_2(x,t) = \frac{V_0}{2}\mathrm{Min}\left[\left(\xi^2 - \frac{\sigma^2}{4}\right), E_0^{\rm b}\cos(\Omega t)\cos(kX_n)\right], \quad (15a)$$

with

$$\begin{aligned} x &= X_n + \xi, \\ X_n &= na_x \quad \text{and} \quad -a_x/2 < \xi < a_x/2, \end{aligned}$$

$$\phi_3(x,t) = \frac{V_0}{2}\mathrm{Min}\left[C(x,t)\left(\xi^2 - \frac{\sigma^2}{4}\right), 0\right], \quad (16a)$$

with

$$\begin{aligned} x &= X_n + \xi, \\ X_n &= na_n \quad \text{and} \quad -a_x/2 < \xi < a_x/2, \\ C(x,t) &= 1 + C_0\cos(\Omega t)\cos(kX_n), \end{aligned} \quad (16b)$$

$$\phi_4(x,t) = \frac{V_0}{2}\mathrm{Min}\left[\left(\xi^2 - \frac{\sigma^2}{4}\right), 0\right], \quad (17a)$$

with

$$\begin{aligned} x &= X_n + u(x,t) + \xi, \\ X_n &= na \quad \text{and} - a/2 < \xi < a/2, \\ u(x,t) &= u_0\cos(\Omega t)\sin(kX_n), \end{aligned} \quad (17b)$$

where σ_0, E_0^b, C_0 and U_0 are parameters.

Quantitatively, the amplitude of modulation of $E^{\rm ad}$ (controlled by the parameter σ_0 Eq. (14b)) and $E_0^{\rm b}$ equation (15a) corresponds to 10% of the diffusion energy barrier, i.e. a value corresponding to the expected modifications of diffusion energy barrier by a strain of 4% for the LJ potential (see Fig. 8b). Note that the modulation of $E^{\rm ad}$ by the longitudinal strain field is expected to be very weak for the Lenard-Jones potential. However, since such modulation is significant for the silver EAM semi-empirical potential, the resolution of equation (12) using the potential $\phi_1(x,t)$ is relevant. The amplitude of the modulation C_0 equation (16b) of the curvature in the potential $\phi_3(x,t)$ is about 6% in agreement with results of Figure 9. And finally, the imposed amplitude u_0 equation (17b) of the displacement field corresponds to a maximum longitudinal strain of 4%. For each case, the wavelength of the modulation is taken to be equal to the StSAW in the MD simulations: $\lambda = 17$ lattice parameter units. $\phi_i(x,t)$ with $i \in \{1,2,3,4\}$ are respectively reported in Figures 10b–10e as a function of x at time $t = 0$. While the modulation of the potential properties are clearly visible for $\phi_1(x,t)$, $\phi_2(x,t)$ and$\phi_4(x,t)$, the one for $\phi_3(x,t)$ asks a closer inspection and a comparison with $\phi_0(x,t)$.

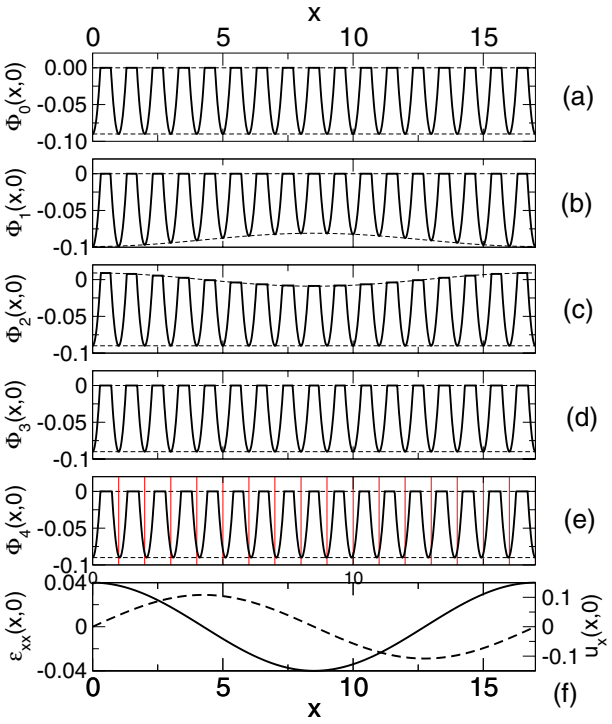

Fig. 10. $\phi_0(x,0)$(a), $\phi_1(x,0)$(b), $\phi_2(x,0)$(c), $\phi_3(x,0)$(d) and $\phi_4(x,0)$(e) as a function of x. Horizontal dashed lines are guides to the eyes to show the modulation or not of maxima or minima of the potentials. Vertical red (grey) solid lines are guides to the eyes to display the modulation of the minima position of $\phi_1(x,0)$. (f) Strain (solid line) $\epsilon_{xx}(x,0)$ and displacement (dashed line) $u_x(x,0)$ field as a function of x.

These crystalline potentials expressions have been chosen in order to be able to uncorrelate the four mentioned modifications of the crystalline potential induced by the StSAW. Values of γ and D in equation (12) have been chosen so that the characteristic time $\tau_{diff}^{Langevin} = 300$ time units[2] of residence (in absence of StSAW) of an adatom in a crystalline potential well is significantly larger than the period $\tau_{self}^{Langevin} = 4.4$ time units of the free oscillation of the adatom in a crystalline potential well. The period of the StSAW is chosen as $T_{StSAW}^{Langevin} = \frac{2\pi}{\Omega} = 50$ time units i.e. a time smaller than the characteristic resident time $\tau_{diff}^{Langevin}$ and larger that the adatom self-oscillation

[2] This quantity has been evaluated by solving equation (12) for $\phi_0(x,t)$ and by calculating and then fitting by a decreasing exponential the distribution of residence time of the adatom in a crystalline potential well.

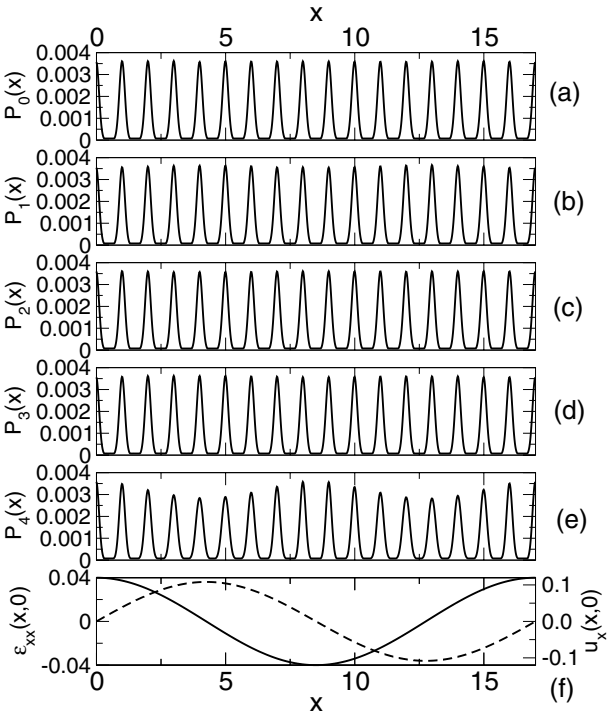

Fig. 11. (a) $P_0(x)$, (b) $P_1(x)$, (c) $P_2(x)$, (d) $P_3(x)$ and (e) $P_3(x)$ as a function of x. (f) Same as Figure 10f.

period $\tau_{self}^{Langevin} = 4.4$. Hence, these different relevant timescales used to solve equation (12) verify:

$$\tau_{self}^{Langevin} = 4.4 \ll T_{StSAW}^{Langevin} = 50 \ll \tau_{diff}^{Langevin} = 300. \quad (18)$$

Note that the ratios between these different timescales are consistent with the ones found during MD simulations:

$$\tau_{self}^{MD} = \frac{2\pi}{\omega_0^x} = 0.79 \ll T_{StSAW}^{MD} = 6.8 \ll \tau_{diff}^{MD} = 50. \quad (19)$$

40 trajectories of 5×10^6 time units are calculated by solving equation (12) with the potentials $\phi_i(x,t)$ with $i \in \{0,1,2,3,4\}$ and with initial conditions evenly spaced along a StSAW wavelength. From these trajectories, the normalized histogram $P_i(x)$ of the x-coordinate of the adatom are calculated and reported in Figure 11. Figure 11f reports the same quantities as Figure 10f. In the following, $\mathfrak{S}_i$ designs the set of the local maxima of $P_i(x)$ with $i \in \{0,1,2,3,4\}$.

In the potential $\phi_0(x,t)$, the adatom performs a Brownian trajectory and the corresponding normalized histogram $P_0(x)$ reported in Figure 11a is an oscillating function (whose period is the lattice parameter) of nearly constant amplitude. Considering the set $\mathfrak{S}_0$ of local maxima of $P_0(x)$ and calculating its average and variance, the relative variance of $\mathfrak{S}_0$ is 0.37%.

The normalized histograms $P_1(x)$ and $P_3(x)$ are oscillating functions (whose periods are the lattice parameter) of nearly varying amplitude. The relative variances of the set $\mathfrak{S}_1$ and $\mathfrak{S}_3$ are 1.03% and 0.6%. However, some weak spatial modulations of the maxima of the oscillation at half the StSAW wavelength are detectable: the amplitudes of these modulations correspond to about 1.6% and 0.9% of the average of $\mathfrak{S}_1$ and $\mathfrak{S}_3$. In addition, these modulations increase (not shown) when increasing the modulation amplitude of the minima E^{ad} of $\phi_1(x,t)$ and of the curvature of $\phi_3(x,t)$. Interestingly, maxima of the amplitude of $P_1(x)$ and $P_3(x)$ coincide with nodes of the strain field. i.e. anti-nodes of the longitudinal displacement field. Indeed, the force induced by the StSAW is in this case proportional to the longitudinal strain field (see Sect. 4.2.1), and the probability to find the adatom is maximum in the vicinity of nodes of the force amplitude [7] corresponding hence to nodes of the longitudinal strain field.

The normalized histogram $P_2(x)$ is an oscillating function (whose period is the lattice parameter) of nearly constant amplitude. The relative variance of the set $\mathfrak{S}_2$ is 0.38% i.e. a value close to the one found when using potential $\phi_0(x,t)$. In addition, no spatial modulation of the maxima of the oscillation at half the StSAW wavelength is measurable. Doubling the modulation amplitude of the maxima E_x^{b} does not change this result. Indeed, the force induced by the StSAW is significant at the top of the crystalline potential barrier where $\phi_2(x,t)$ and $\phi_0(x)$ significantly differ (see Sect. 4.2.1). Since the adatom spends most of its time in the vicinity of minima of the crystalline potential, the adatom only barely feels this force induced by the StSAW.

The normalized histogram $P_4(x)$ is an oscillating function (which period is the lattice parameter) whose amplitudes are significantly spatially modulated at half the StSAW wavelength: the amplitude of this modulation corresponds to about 12% of the average value of the set $\mathfrak{S}_4$. Maxima of the amplitude of $P_4(x)$ correspond to nodes of the longitudinal displacement field. Indeed, the force induced by the StSAW is in this case proportional to the longitudinal displacement field (see Sect. 4.2.3), and the probability to find the adatom is maximum in the vicinity of nodes of the force [7] corresponding hence to nodes of the longitudinal displacement.

Comparing the different exhibited structuring mechanisms, the modulation of 4% of the minima positions of the crystalline potential ($\phi_4(x,t)$) by the StSAW induces a significantly larger structuring effect than others. We then conclude that the modulation of the minima positions of the crystalline potential by the StSAW is the dominant StSAW force generation mechanism and the probability to find the adatom in the vicinity of a node of the longitudinal displacement is maximum in agreement with MD simulations results.

In the case of MD simulations using a Lenard-Jones potential, since minima of the crystalline potential weakly depend on the strain field of the StSAW, only the inertial and curvature effects are active while using an EAM potential, the three mentioned structuring mechanisms are active. However, for both potential, the inertial effect dominates inducing a maximum probability to find the adatom in the vicinity of a node of the longitudinal displacement, i.e. following equation (10) in the vicinity of an anti-node of the transverse surface displacement, as observed in the MD simulations [4].

5 Relation between the force $F_{StSAW}(x,t)$ induced by the StSAW and the force $F_{tot}(x,t)$ acting on the adatom

The force $F_{acc}(x,t)$ evaluated in Section 3.2 takes into account both the static force $F_{StSAW}(x,t)$ induced by the StSAW and the response of the adatom to this force in the crystalline potential.

In order to uncover the relation between these two forces, the unidimensional model of the adatom already mentioned is used [6].

The adatom position x is solution of equation (12)

$$\ddot{x} + \gamma\dot{x} = -\frac{\partial\phi_4(x,t)}{\partial x} + \zeta(t), \tag{20}$$

where only the dominant StSAW force generation mechanism is considered with the potential $\phi_4(x,t)$. While evaluating the force $F_{acc}(x,t)$ in MD simulations, the adatom remains in a crystalline potential well. Hence the crystalline potential $\phi_4(x,t)$ can be developed at the first order in displacement in the vicinity of a crystalline potential minimum. Using equations (17) and (20) writes:

$$\ddot{x} + \gamma\dot{x} + V_0(x - X_n) = V_0 u_0 \cos(\Omega t)\sin(kX_n) + \zeta(t) \tag{21}$$

with

$$x = X_n + u(x,t) + \xi$$
$$X_n = na_x \quad \text{and} \quad -a_x/2 < \xi < a_x/2.$$

Note that an analog equation would be obtained for any realistic crystalline potential modelled by its harmonic approximation in the vicinity of one of its minima, V_0 then corresponding to the square of the eigenfrequency ω_0^x of the adatom in a unperturbed potential well: $V_0 = (\omega_0^x)^2$. From equation (21), the static force simply writes here: $F_{StSAW}(x,t) = F^0_{StSAW}\cos(\Omega t)\sin(kX_n)$ with $F^0_{StSAW} = V_0 u_0$.

Equation (20) can be easily solved. The solution of equation (20) in the vicinity of a potential minimum then reads:

$$x(t) = X_n + \frac{F^0_{StSAW}}{\sqrt{(\Omega^2 - (\omega_0^x)^2)^2 + \gamma^2\Omega^2}}\sin(kX_n)\cos(\Omega t - \varphi) + \int_{t_0}^{t}\zeta(t')G(t-t')dt', \tag{22}$$

where

$$\tan\varphi = -\frac{\gamma\Omega}{\Omega^2 - (\omega_0^x)^2}.$$

$G(t)$ is the Green function of the left hand side of equation (21):

$$G(t) = \frac{e^{-\frac{\gamma t}{2}}\sin(\omega_r t)}{\omega_r} \quad \text{with} \quad \omega_r = \sqrt{(\omega_0^x)^2 - \frac{\gamma^2}{4}}.$$

For any realistic situation, γ is small compared to ω_0^x: the characteristic time of transfer of energy from the adatom to the substrate is large compared to a self-oscillation period of an adatom in a unperturbed crystalline potential well so $\gamma \ll \omega_0^x$. Moreover, noting that $\Omega^2 \ll (\omega_0^x)^2$, $\varphi \approx 0$ and the position $x(t)$ of the adatom approximately writes:

$$x(t) \approx X_n + \frac{F^0_{StSAW}}{(\omega_0^x)^2}\sin(kX_n)\cos(\Omega t) + \int_{t_0}^{t}\zeta(t')G(t-t')dt'. \tag{23}$$

The measured force $F_{acc}(x,t)$ in Section 3.2 is proportional to the Fourrier component at the StSAW frequency of the acceleration of the adatom so that:

$$F_{acc}(x,t) = -\frac{F^0_{StSAW}\Omega^2}{\omega_0^2}\sin(kX_n)\cos(\Omega t) = -\frac{\Omega^2}{(\omega_0^x)^2}F_{StSAW}(x,t). \tag{24}$$

Equation (24) establishes the relation between the force $F_{StSAW}(x,t)$ equation (6) induced by the StSAW discussed in Section 4.2 and the force $F_{acc}(x,t)$ equation (3) measured during the MD simulations in Section 3.2.

Equation (24) evidences the proportionality between $F_{StSAW}(x,t)$ and $F_{acc}(x,t)$ so that:

$$F^0_{acc} = -F^0_{StSAW}\frac{\Omega^2}{\omega_0^2}. \tag{25}$$

6 Parameters effect

In this section, the influence of the amplitude, frequency, direction of the StSAW and of the substrate temperature in the MD simulations are investigated.

6.1 StSAW amplitude and frequency

This section reports the dependence of the structuring effects on the StSAW amplitude and frequency.

6.1.1 Force and StSAW amplitude

MD simulations of the adatom diffusing in the presence of the StSAW are performed changing the amplitude of the substrate atoms displacement generating the StSAW, which also equals the StSAW transverse displacement amplitude equation (10b). This amplitude is limited in order to avoid any plastic deformation or loss of crystallinity in the substrate.

For each investigated amplitude A, the amplitude F^0_{acc} of the force $F_{tot}(x,t)$ equation (3) acting on the adatom is measured following the procedure described in Section 3.2.

Figure 12a reports the values of F^0_{acc} (in LJ units) as a function of the amplitude A of the StSAW transverse displacement field for three different StSAW frequencies. $\Omega = 1.68$, $\Omega = 0.924$ and $\Omega = 0.702$. For all values of Ω, the amplitude F^0_{acc} of the force acting on the adatom,

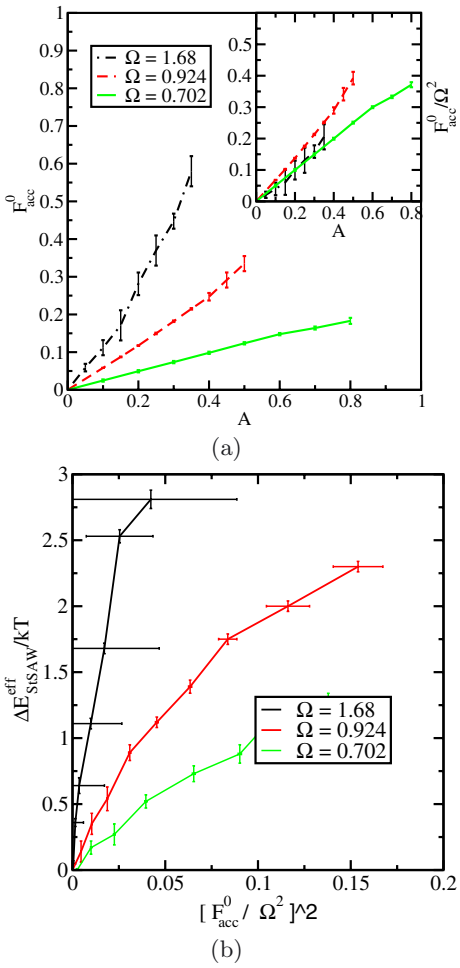

Fig. 12. (a) Amplitude F^0_{acc} of the force acting on the adatom as a function of the amplitude A of the StSAW transverse displacement field. Calculations are performed for $\Omega = 1.68, 0.924$ and 0.702 using the same procedure as part 3.2. The inset reports the ratio $\frac{F^0_{acc}}{\Omega^2}$ as a function of the amplitude A. (b) $\Delta E^{\text{eff}}_{StSAW}$ as a function of the squared amplitude of the force. The substrate temperature is $T = 0.24$. The StSAW is propagating along the [110] direction on the (001) surface with parameters: for $\lambda = 9\ a_x$, $A = 0..0.35$, $\Omega = 1.68$, for $\lambda = 17a_x$, $A = 0..0.5$, $\Omega = 0.924$ and for $\lambda = 34a_x$, $A = 0..0.8$, $\Omega = 0.702$.

with a good approximation, linearly varies with the amplitude A of the StSAW. Indeed, in Section 4.3, inertial effects have been shown to be the dominating mechanism yielding the structuration: the force $F_{StSAW}(x,t)$ is hence expected to be proportional to the longitudinal displacement field. From equations (10a), (10b) and (24), we thus deduce that the amplitude F^0_{acc} of the force $F_{tot}(x,t)$ is proportional to the amplitude A of the transverse displacement fields and to the StSAW frequency square. Figure 12a confirms the linearity of F^0_{acc} with the amplitude A. The linearity of F^0_{acc} with the StSAW frequency square is revealed by inset of Figure 12a reporting the values of $\frac{F^0_{acc}}{\Omega^2}$ as a function of the StSAW amplitude A: the 3 curves obtained for different frequencies are approximately super-imposed.

The good agreement between the theoretical analysis and results of Figure 12 evidences the relevance of our analysis showing that inertial effects are mainly responsible of the structuration.

6.1.2 Structuring energy and force

In reference [4], the structuring energy $\frac{\Delta E^{\text{eff}}_{StSAW}}{kT}$ has been shown to depend on the square of the amplitude of the force $F^0_{StSAW} = \frac{F^0_{acc}\omega_0^2}{\Omega^2}$ (Eq. (25)).

For each value of the amplitude A of the StSAW transverse displacement field, a set of adatom trajectories are performed by MD simulations. The normalized histograms $P(x)$ are calculated from which the structuring energies $\Delta E^{\text{eff}}_{StSAW}$ are deduced. Figure 12b reports $\Delta E^{\text{eff}}_{StSAW}$ as a function of $[\frac{F^0_{acc}}{\Omega^2}]^2$.

The linear relationship between $\Delta E^{\text{eff}}_{StSAW}$ and $[\frac{F^0_{acc}}{\Omega^2}]^2$ (at given Ω) is nearly verified in the range 0 to 0.05 square-(force-time) units. Above this limit, the non-linearities are more pronounced. The linear relation between the structuring energy $\frac{\Delta E^{\text{eff}}_{StSAW}}{kT}$ and the square of the amplitude of the force F^0_{StSAW} originates from a perturbation theory calculations at the first order for the adatom displacement [7], only relevant for small adatom displacements.

In the linear regime, if actually $\Delta E^{\text{eff}}_{StSAW}$ scales as the square of $F^0_{StSAW} = \frac{F^0_{acc}\omega_0^2}{\Omega^2}$, the structuring energy $\Delta E^{\text{eff}}_{StSAW}$ has an additional dependence on the StSAW frequency. To our knowledge, no theoretical expression of the structuring effect taking into account all the system complexity and able to fully describe $\Delta E^{\text{eff}}_{StSAW}$ is available. Such theoretical expression is still missing and is far out of the scope of the present manuscript.

6.2 Direction of the wave vector

In reference [4], the structuring energy induced by a StSAW on a (001) crystal surface propagating in the [100] direction has been reported. Here, the effect of StSAW propagating in the [110] direction on a (001) crystal surface has been studied. Figure 13 reports the distribution $P(x)$ of adatoms position for both cases. To only investigate the effect of the wave vector direction, in both cases, the frequency of the StSAW and the substrate amplitude displacement have been chosen to be as close as possible: $A = 0.4$, $\Omega = 0.904$, $\lambda = 38.08$ for the StSAW along the [100] direction; $A = 0.4$, $\Omega = 0.924$, $\lambda = 38.16$ for the StSAW along the [110] direction.

The measure of the structuring energies gives: $\Delta E^{[100]}_{StSAW} = 1.21 k_B T$ and $\Delta E^{[110]}_{StSAW} = 1.55 k_B T$ for wave vectors along the [100] and [110] directions respectively. The structuring effect of the StSAW is thus slightly more pronounced for a wave vector along the [110] direction than for a wave propagating in the [100] direction. This difference could be related to the different diffusion mechanism in both directions. Figure 2 illustrates a top

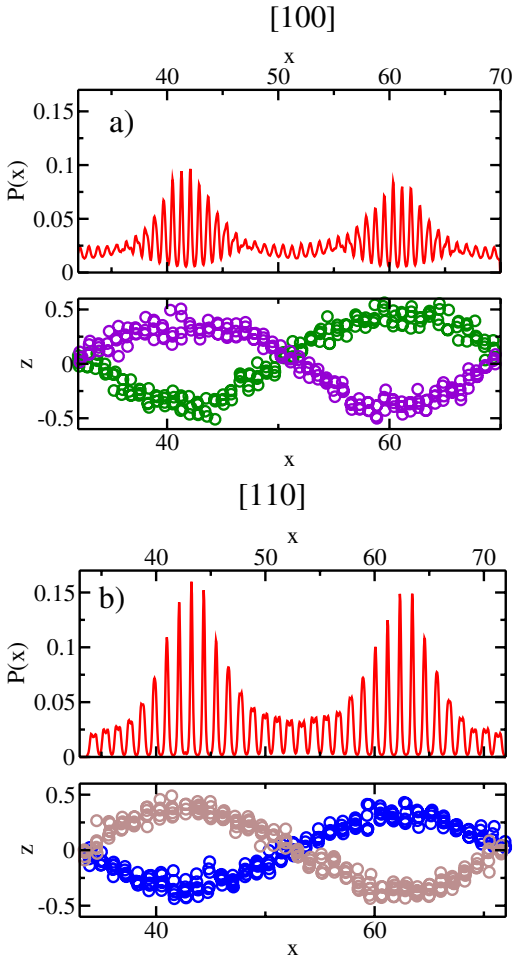

Fig. 13. Distribution $P(x)$ of adatoms position on a (001) substrate surface with a StSAW propagating along the (a) [100] and (b) [110] direction. In both cases, the transverse substrate displacement is reported (same as Fig. 2c). Distributions are calculated from 200 independent trajectories of 8000 time units long with initial conditions evenly spread along one wavelength of the StSAW. Simulations are performed using a Lennard-Jones interaction potential at the substrate temperature $T = 0.24$. The StSAW parameters are: $A = 0.4$, $\Omega = 0.904$, $\lambda = 38.08$ for the StSAW along the [100] direction; $A = 0.4$, $\Omega = 0.924$, $\lambda = 38.16$ for the StSAW along the [110] direction.

view of the (001) crystal surface with a StSAW propagating along the [100] and [110] directions. The diffusion along the [110] direction is straight: the diffusion along the [110] direction and along the $[\bar{1}10]$ direction involve some uncorrelated elementary mechanisms. The diffusion along the [100] direction is performed through a zig-zag shape enlightened in Figure 2 and thus involves the same elementary mechanisms as the diffusion along the [010] direction. This difference of diffusion mechanism is also revealed by the near null and finite values of minima of the distribution $P(x)$ for a StSAW along the [110] and along the [100] directions: the probability to find the adatom at a bridge site position of the crystalline potential is significantly higher for StSAW propagating along the [100] direction than along the [110] direction.

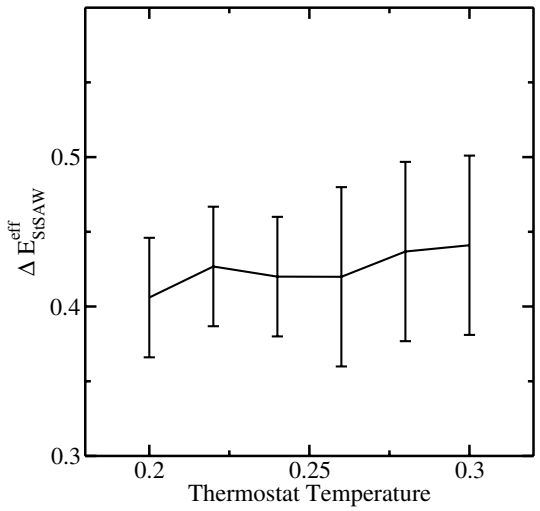

Fig. 14. $\Delta E^{\text{eff}}_{StSAW}$ as a function of the temperature of the thermostat. Statistics are made over 200 independent trajectories with initial condition evenly spread along one wavelength of the StSAW for a range of thermostat temperature from $T = 0.2$ to $T = 0.3$. The StSAW is propagating along the [110]direction on the (001) surface with parameters: $\lambda = 17a_x$, $A = 0.4$, $\Omega \approx 0.924$ but slightly depends on the temperature.

6.3 Temperature dependence of the structuration

The dimensionless structuring energy $\Delta E^{\text{eff}}_{StSAW}/kT$ is calculated for different substrates temperatures ranging from $T = 0.2$ to $T = 0.3$. The angular frequency of the applied StSAW is about $\Omega \approx 0.924$ but slightly depends on the temperature due to the anharmonic terms in the LJ potentials. The available range of temperature is rather small: below $T = 0.2$, the diffusion is too slow to get good statistics performing reasonable simulations runs with regards to our computational facilities. Beyond $T = 0.3$, the adatom evaporation is too frequent to reach a reasonable statistics. Figure 14 reports the structuring energy $\Delta E^{\text{eff}}_{StSAW}$ as a function of the substrate temperature. $\Delta E^{\text{eff}}_{StSAW}$ is roughly independent on the temperature. The temperature has a disordering effect and competes the structuring effect induced by the StSAW. As a net result, the dimensionledd structuring energy $\Delta E^{\text{eff}}_{StSAW}/kT$ that both accounts for the StSAW and the thermal noise, is a decreasing function of the temperature. To our knowledge, no analytical expression are currently able to describe this temperature dependence.

7 Conclusion

We have shown that a StSAW can govern the diffusion of adatoms on a substrate surface: the anti-nodes of the substrate transverse displacements are some preferential sites where the adatoms have a better chance to be observed.

The mechanism leading to this structuring effect relies on the fact that the crystalline potential seen by the adatom is modulated by the StSAW. This modification of the crystalline potential induces a static force F^0_{StSAW}

on the adatom. The effects of the StSAW have been analysed by measuring the instantaneous force F^0_{acc} acting on the adatom. Such a force has been related to the static force F^0_{StSAW} induced by the StSAW.

Four main modifications of the crystalline potential have been considered: among them, we have shown that inertial effect is the main mechanism responsible of the structuring effect within the conditions of the MD simulations.

The structuring effect has been shown to quadratically vary on the excitation, to depend on the wave-vector directions and to decrease with temperature. This study confirms the influence of a StSAW on the adatom diffusion and quantifies the structuring effect dependence on the amplitude, frequency and wave vector directions of the StSAW and on the temperature.

From this study, we can reasonably expect that several adatoms present on a substrate submitted to a StSAW will aggregate to form self-organized nanostructures. The effects of the StSAW on the diffusion of several adatoms and of aggregates is currently studied and will be reported in a forthcoming publication.

This structuration technique has not been experimentally investigated yet: both the creation of short wavelengths Surface Acoustic Wave (SAW) and their introduction in a growth chamber constitutes technical challenges. However, though the creation of a SAW with very small wavelength is difficult [18,19], recent results report the possibility to generate a SAW with a wavelength of 45 nm [20]. In our study, typical wavelengths are about $17a_x$ i.e. of the order of 10 nm (assuming $a = 0.4$ nm): hence, state-of-the-art SAWs have wavelengths about 4 times longer that the ones used in this study. Besides, a strong enhancement of the surface diffusion of adatom by SAW has been experimentally evidenced very recently [21]. So technically challenging, we are confident that experimental investigations of the dynamical structuring effects will soon be considered at the atomic scale knowing that a similar technique is currently widely used using μm wavelength pressure wave in fluid media to self-organized objects [22,23].

Finally, the dynamical structuring effects is very versatile since using several StSAWs, square or triangular 2D networks could be obtained at the nanoscale: the number, wave vectors direction [19,22], and wavelengths of SAW control the position and density of nanostructures.

We believe that this method might be a fast, elegant and alternative way to elaborate nano-components.

This work was performed using HPC resources from CALMIP (Grant 2010-1022]).

References

1. H. Brune, M. Giovannini, K. Bromann, K. Kern, Nature **394**, 451 (1998)
2. G. Jin, J.L. Liu, S.G. Thomas, Y.H. Luo, K.L. Wang, B.Y. Nguyen, Appl. Phys. Lett. **75**, 2752 (1999)
3. A. Zangwill, *Physics at surface* (Cambridge University Press, Cambridge, 1988)
4. C. Taillan, N. Combe, J. Morillo, Phys. Rev. Lett. **106**, 076102 (2011)
5. I.S. Aranson, L.S. Tsimring, Rev. Mod. Phys. **78**, 641 (2006)
6. N. Combe, C. Taillan, J. Morillo, Phys. Rev. B **85**, 155420 (2012)
7. C. Taillan, N. Combe, J. Morillo, Phys. Rev. B **85**, 155421 (2012)
8. S.J. Plimpton, J. Comp. Phys. **117**, 1 (1995)
9. L.D. Landau, E.M. Lifshitz, *Theory of elasticity* (Pergamon Press, Oxford, 1986)
10. Y.X. Wang, Z.Y. Pan, Z.J. Li, Q. Wei, L.K. Zang, Z.X. Zhang, Surf. Sci. **545**, 137 (2003)
11. L. Gammaitoni, P. Hänggi, P. Jung, F. Marchesoni, Rev. Mod. Phys. **70**, 223 (1998)
12. D. Royer, E. Dieulesaint, J. Acoust. Soc. Am. **76**, 1438 (1984)
13. C. Ratsch, A.P. Seitsonen, M. Scheffler, Phys. Rev. B **55**, 6750 (1997)
14. M. Schroeder, D.E. Wolf, Surf. Sci. **375**, 129 (1997)
15. G. Henkelman, B.P. Uberuaga, H. Jonsson, J. Chem. Phys. **113**, 9901 (2000)
16. C. Taillan, Ph.D. thesis, Université de Toulouse, France, 2012
17. C. Wu, V.Y. Zaitsev, L.V. Zhigilei, Appl. Phys. Lett. **103**, 221601 (2013)
18. M.E. Siemens, Q. Li, M.M. Murnane, H.C. Kapteyn, R. Yang, E. Anderson, K.A. Nelson, Appl. Phys. Lett. **94**, 093103 (2009)
19. T. Sogawa, H. Gotoh, Y. Hirayama, P.V. Santos, K.H. Ploog, Appl. Phys. Lett. **91**, 141917 (2007)
20. Q. Li et al., Phys. Rev. B **85**, 195431 (2012)
21. M.V. Shugaev, A.J. Manzo, C. Wu, V.Y. Zaitsev, H. Helvajian, L.V. Zhigilei, Phys. Rev. B **91**, 235450 (2015)
22. J. Shi, D. Ahmed, X. Mao, S.C.S. Lin, A. Lawita, T.J. Huang, Lab. Chip **9**, 2890 (2009)
23. Y. Chen, X. Ding, S. Steven Lin, S. Yang, P.H. Huang, N. Nama, Y. Zhao, A.A. Nawaz, F. Guo, W. Wang, Y. Gu, T.E. Mallouk, T.J. Huang, ACS Nano **7**, 3306 (2013)